frontiers in Energy Research

BRIEF RESEARCH REPORT
published: 13 January 2022
doi: 10.3389/fenrg.2021.815633

Preparation of Mn/Mg/Ce Ternary Ozone Catalyst and Its Mechanism for the Degradation of Printing and Dyeing Wastewater

Shuai Zhang[1], *Huixue Ren*[1,2]*, *Kaifang Fu*[1,2], *Wenqing Cheng*[1], *Daoji Wu*[1,2], *Congwei Luo*[1,2], *Shengyun Jiang*[1], *Jie Li*[1] *and Mingyue Zhang*[1]

[1]School of Municipal and Environmental Engineering, Shandong Jianzhu University, Jinan, China, [2]Institute of Resources and Environment Innovation, Shandong Jianzhu University, Jinan, China

The printing and dyeing wastewater produced by different dyes, as well as different printing and dyeing processes, have different components. These wastewater have high toxicity, high organic concentration, and deep chromaticity. Ozone catalytic oxidation is a very promising technical method for wastewater treatment. In this paper, Mn/Mg/Ce ternary catalyst was prepared, and the ozone catalytic oxidation treatment of actual and simulated printing and dyeing wastewater was performed to study the performance of four different carrier catalysts, namely, molecular sieve (MS), silica gel (SG), attapulgite (ATP), and nano alumina (Al_2O_3), by simulated dynamic test. The effects of reaction time, pH, and catalyst dosage on methyl orange degradation were studied. The results showed that under the optimum treatment conditions (120 min, pH 11, and 12.5 g/L catalyst dosage), the degradation rate of methyl orange reached 96% and the removal rate of the chemical oxygen demand of printing and dyeing wastewater reached 48.7%. This study shows that the treatment effect of ozone catalytic oxidation on printing and dyeing wastewater is remarkably improved after catalyst addition. This study provides a new choice of ozone catalyst for the degradation of printing and dyeing wastewaters in the future.

Keywords: ozone catalysis, ternary catalyst, printing and dyeing wastewater, degradation, mechanism

OPEN ACCESS

Edited by:
Xinqi Chen,
Hubei University of Education, China

Reviewed by:
Qi Yang,
China University of Geosciences, China
Ming-Guo Ma,
Beijing Forestry University, China

***Correspondence:**
Huixue Ren
renhx138@163.com

Specialty section:
This article was submitted to Electrochemical Energy Conversion and Storage, a section of the journal Frontiers in Energy Research

Received: *15 November 2021*
Accepted: *16 December 2021*
Published: *13 January 2022*

Citation:
Zhang S, Ren H, Fu K, Cheng W, Wu D, Luo C, Jiang S, Li J and Zhang M (2022) Preparation of Mn/Mg/Ce Ternary Ozone Catalyst and Its Mechanism for the Degradation of Printing and Dyeing Wastewater. Front. Energy Res. 9:815633. doi: 10.3389/fenrg.2021.815633

INTRODUCTION

Printing and dyeing wastewater often have high toxicity, high chromaticity, many organic pollutants, and difficult degradation. High chromaticity affects light transmission in water, and organic pollutants consume dissolved oxygen in water, which results in water body destruction and affects the living environment of aquatic organisms. Printing and dyeing wastewater are difficult to treat, and general physical and chemical treatments have difficulty in achieving good results (Kawasaki et al., 2012; Hayat et al., 2021; Lun et al., 2021).

As an efficient and clean advanced oxidation technology, ozone uses the large number of strong oxidizing free radicals produced in the reaction process to oxidize organic matter in water to achieve water purification. The application of ozone catalytic oxidation technology in printing and dyeing wastewater has gradually matured (Takahashi et al., 2012; Mirilă et al., 2020; Tabrizi et al., 2011). The problems of this technology include low oxygen oxidation efficiency and low utilization rate. Ozone catalyst can improve the mass transfer efficiency and utilization of ozone and shorten the reaction time (Zhang et al., 2021; Mansouri et al., 2013). Under optimum conditions, the chemical oxygen

demand (COD) removal efficiency can reach 96.3% in the catalytic ozonation of oil refining wastewater with alumina-supported manganese and copper oxides (Deng et al., 2015; He et al., 2021; Jiang et al., 2021). The COD removal rate reached 96% after 120 min when iron and nickel foam was used as the catalyst to catalyze the ozonation of organic pollutants in actual petrochemical wastewater. The contents of total phosphorous, total nitrogen, NO_3–N, Cl^-, and some heavy metals in petrochemical wastewater were also eliminated to a certain extent (Huang et al., 2018). Iron-based catalysts remarkably improve the mineralization of organic pollutants in coking wastewater. The removal rate of total organic carbon is very high and can reach 78.7% (Li et al., 2017; Feng et al., 2021). Research on rare Earth elements as ozone catalyst on actual industrial wastewater has become increasingly mature (Jeirani and Soltan 2016). Cerium ions can be transformed between trivalent and tetravalent states to achieve electron transfer because of its special 4f orbit and high catalytic activity (Akhtar et al., 2011; Martins and Quinta-Ferreira 2009). Under heterogeneous catalytic conditions, CE/AC can promote the conversion of ozone to hydroxyl radical, which can greatly improve the degradation rate of TSA and the efficiency of ozone oxidation to remove COD (Dai et al., 2014; Zuo et al., 2021). Ozone catalyst is increasingly used in the treatment of printing and dyeing wastewater, but it still has limitations in actual application. The mass transfer efficiency of ozone can be improved by increasing microbubble generation in the reactor to reduce the volume of ozone bubbles and increase hydraulic retention time.

ATP is a cheap and resource-rich natural hydrated magnesium aluminum silicate clay mineral. Owing to its desirable properties-such as a large specific surface area and micro- and mesoporous structure, ATP is widely used as an adsorbent in various industries (Cui et al., 2013; Liu and Guo 2006). Al_2O_3 has been widely used as a catalyst carrier due to its large specific surface area, decent stability, uncomplex preparation process and low-cost ingredients, Al_2O_3 as a carrier has a good ability for catalytic dehydrogenation and ozone catalysis (Chen et al., 2021; Bataklieva et al., 2015). MS material can absorb most of the visible light through its unique surface acidity and anionic framework structure, which can be used as the eligible support for photocatalyst, MS as desiccant can better absorb the impregnation solution and improve the load of impregnation elements (Bian et al., 2020). SG may be a better carrier for the following qualities: it is an amorphous inorganic polymer composed of siloxane groups (Si-O-Si) in the framework and silanol groups (Si-OH) on the surface which can be easily functionalized by chemical modification; moreover, it is biocompatible and biologically inert (Zhang et al., 2007). To sum up, this paper selects the above four different carriers to load the target elements to make catalysts. Through experimental characterization and results, observe the removal effect of different catalyst carriers on printing and dyeing wastewater and explore its influence mechanism.

In this work, supported Mn/Mg/Ce catalysts were prepared by an incipient wetness impregnation procedure followed by drying and calcination in a muffle furnace. The preparation conditions and process conditions were optimized. The structure and physicochemical properties of the catalysts were characterized by scanning electron microscopy (SEM), Fourier transform infrared (FTIR) spectroscopy, and Brunauer–Emmett–Teller (BET) surface area analysis. The heterogeneous catalytic ozonation system used in the experiment consists of microbubble ozone.

MATERIALS AND METHODS

Catalyst Preparation

The ternary catalyst was prepared by impregnation and calcination. Manganese nitrate solution (10%), magnesium nitrate solution (5%), and cerium nitrate solution (5%) were dissolved and mixed to the volume ratio of 2:5:1. Attapulgite (17 g), alumina (17 g), molecular sieve (17 g) and silica gel (17 g) were added to independent 250 ml impregnation solution respectively and placed on a shaking table for 12 h at 25°C. Afterward, the conical flask was taken out and soaked for 12 h to load metal elements on the attapulgite surface. The catalyst was poured out from the mother liquor and dried in an oven at 80°C. The dried precursor was calcined in the muffle furnace at 500°C for 6.5 h, and the Mg/Mn/Ce catalyst supported on attapulgite was obtained.

Wastewater and Reagents

Two kinds of wastewater were used in the experiment. One is the printing and dyeing wastewater actually produced by Penglai Jiaxin dye Co., Ltd., with COD of 39,000 mg/L, pH = 7.2, NH_4-N = 46 mg/L, BOD = 11523 mg/L. The other is methyl orange wastewater configured in the laboratory, with a concentration of 100 mg/L.

Methyl orange was purchased from Tianjin Hengxing Chemical Reagent Manufacturing Co., Ltd. Manganese nitrate solution (50%), anhydrous magnesium sulfate, and cerium carbonate were purchased from Shanghai McLean Chemical Reagent Manufacturing Co., Ltd. Tertiary butyl alcohol (TBA), MS, Al_2O_3, ATP, and SG were purchased from Shanghai Aladdin Biochemical Technology Co., Ltd. The ozone generator was purchased from Qingdao Meister Purification Equipment Co., Ltd. Except for the marked concentration, the purity of the above reagents are analytical grade.

Characterization of Catalysts

The microscopic morphology of the catalysts were observed using a field-emission scanning electron microscope (JSM-7610F Plus, Jeol, Japan).The loading content of target elements was detected by EDS (GENESIS XM, United States) energy spectrum in SEM. The specific surface areas of the catalysts were measured using a fully automated rapid surface to porosity analyzer (Autosorb iQ, Quantachrome, United States). The functional groups and molecular structure of the catalyst were analyzed using a FTIR spectrometer (TENSOR II, Bruker, Germany). The concentration of liquid-phase ozone in the reactor was measured by a dissolved ozone tester (DOZ30, United States). The molecular packing of

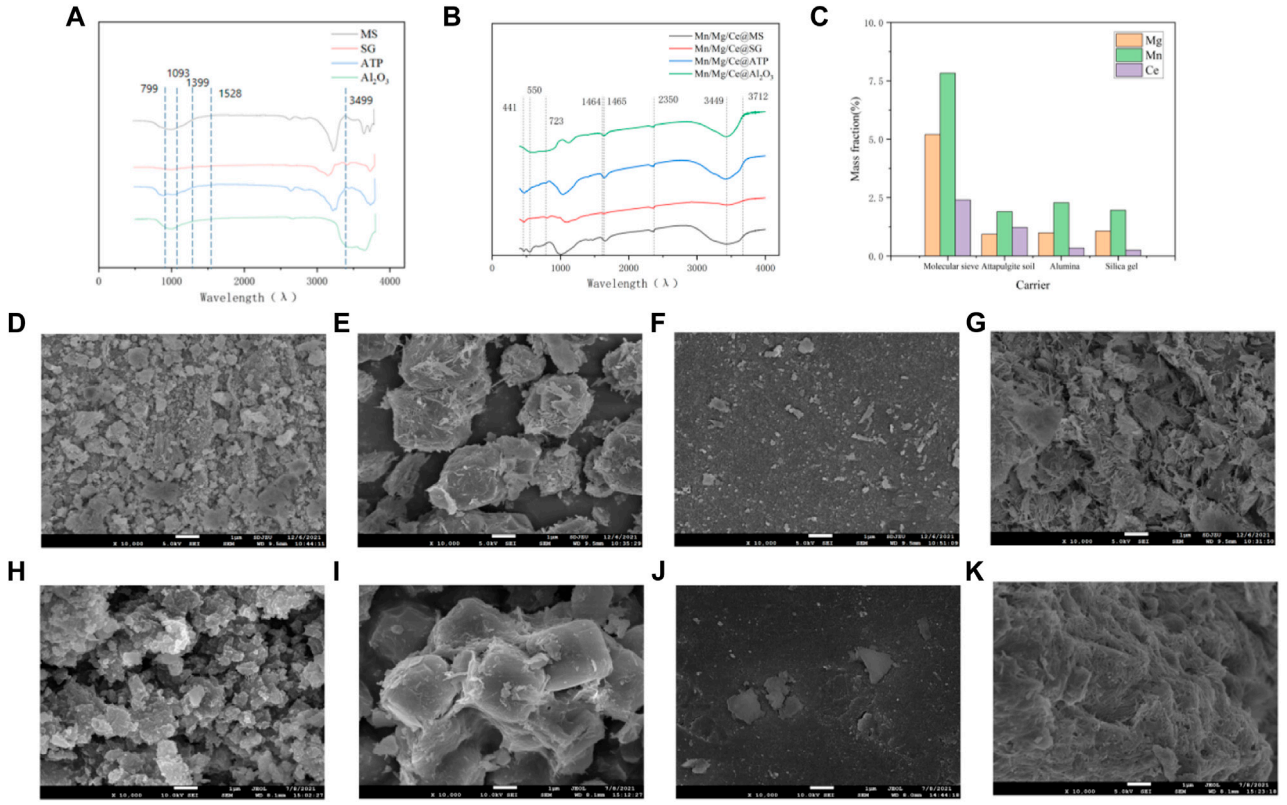

FIGURE 1 | (A) FTIR spectra of the four carriers. **(B)** FTIR spectra of the four catalysts. **(C)** Mass fractions of the target elements loaded by the four carriers. SEM images of **(D)** Al_2O_3, **(E)** MS, **(F)** SG, and **(G)** ATP. **(H)** Mn/Mg/Ce@Al_2O_3, **(I)** Mn/Mg/Ce@MS, **(J)** Mn/Mg/Ce@SG, **(K)** Mn/Mg/Ce@ATP.

the catalysts was analyzed with an XRD-BRUKER D8 ADVANCE powder diffractometer using Cu Kα X-ray radiation. XRD analysis was performed on a rotating X-ray diffractometer in the 2θ range of 5–90°C.

Experimental Methods

The ozone reactor consists of a self-made plexiglass reactor. The right reactor has a height of 300 mm and a diameter of 100 mm. A 2 mm-diameter stainless steel porous dispersion network was installed at the height of 80 mm. The gas distribution device is the aeration plate at the bottom of the reactor. The reactor has a height of 400 mm and a diameter of 100 mm. All experiments were carried out at room temperature. Two liters of reaction wastewater was poured into the right reactor. The cooling water pump, air pump switch, and ozone switch were turned on consecutively in that order. The ozone switch was turned on 1–2 min after the air pump switch was turned on. The effects of different conditions (i.e., reaction time, pH, and catalyst dosage) on the catalytic effect were studied. pH changed slightly during the experiment because hydroxide was consumed in the ozone-catalyzed oxidation reaction. NaOH and H_2SO_4 (1 mol/L) were used to control the pH. Samples were obtained at 30, 60, 90, and 120 min to measure the degradation rate of methyl orange wastewater and the COD of the printing and dyeing wastewater.

RESULTS AND DISCUSSION

Characterization of Catalysts

Figure 1A shows the FTIR spectra of the four catalysts. The characteristic peak at 550 cm^{-1} belongs to MnO_2; the characteristic peaks at 467, 799, 1,093, and 3,449 cm^{-1} belong to SiO_2; and the characteristic peaks at 1,399 and 1,528 cm^{-1} belong to Al_2O_3. **Figure 1B** shows the FTIR spectra of the four catalysts. The characteristic peak at 550 cm^{-1} belongs to MnO_2; the characteristic peaks at 3,712, 1,465, and 435 cm^{-1} belong to MgO; and the characteristic peaks at 1,464, 723, and 441 cm^{-1} belong to CeO_2. Changes in peak value (weakened or shifted) may be related to load and crystallization effects. These characteristic peaks appear in the spectrum, but the intensity and position of the characteristic peaks fluctuate, which may be related to the load and crystallization effect. In **Figure 2C**, it can be seen that the load of Mg, Mn and Ce is less than 10%, and the element load is small, which makes the intensity of the characteristic peaks in the diagram weak. Poor crystallization effect after roasting will make the position of the characteristic peaks fluctuate. This provides a reference for subsequent XRD analysis. The FTIR images of the carriers and catalysts showed that the target element was successfully loaded on the carrier. The FTIR images of the carrier and catalyst showed

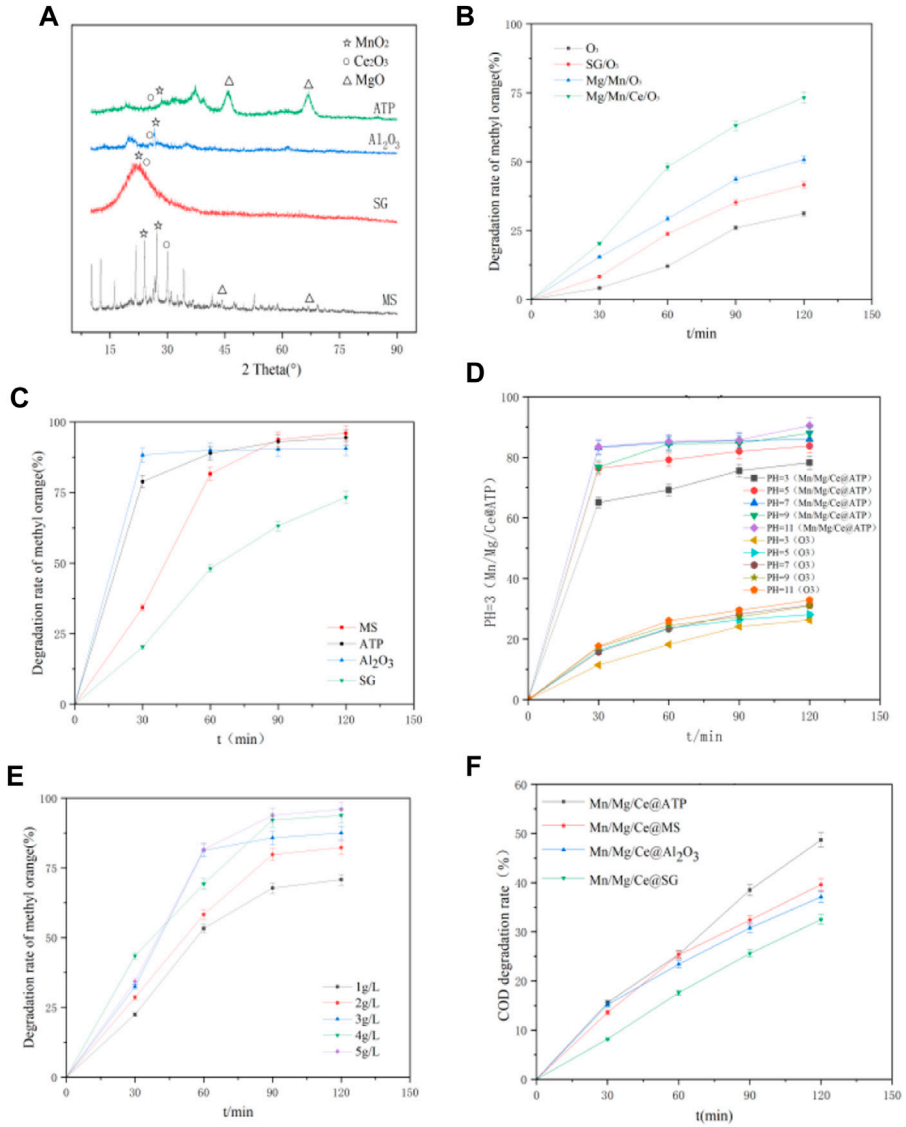

FIGURE 2 | (A) XRD spectrum of four catalysts. Effects of **(B)** impregnation solution, **(C)** carrier, **(D)** pH, and **(E)** catalyst dosage on catalytic performance. **(F)** COD degradation rate of the four catalysts with different supports for red powder wastewater treatment.

that the target element was successfully loaded on the carrier (Prabaharan et al., 2016; Madzokere and Karthigeyan, 2017).

The SEM images of the four carriers catalysts with a magnification of ×10,000 is shown in **Figure 1**. The surfaces of the four materials show different morphological characteristics. It can be seen from **Figures 1D,H** that the surface of alumina is irregular small particles, and the calcined alumina catalyst shows ellipsoid, and the particles are more compact. As shown in the **Figures 1E,I** that after MS roasting, it is a more regular cube, and the small cube is composed of flake structure and has the characteristics of layered structure. In contrast, **Figures 1F,J** show a different type of microstructure, that the surface of SG is smooth and there are obvious load marks on the surface after roasting; The SEM of ATP carrier before and after loading active elements are more characteristic, as shown in the **Figures 1G,K** that the surface of ATP is covered with rod-shaped particles and presents fine fibrous shape after roasting. In particular, when these microstructures are combined with BET results, it can be clearly obtained that the specific surface area and surface properties of the four calcined catalysts were improved.

In addition to the main elements of the catalysts (i.e., aluminum and calcium), the contents of the target elements are shown in **Figure 1C**. The element mass fractions of Mg, Mn, and Ce are 5.20, 7.83, and 2.63%, respectively, in the molecular sieve support; 0.93, 1.90, and 1.22%, respectively, in the attapulgite support; 0.99, 2.28, and 0.34%, respectively, in the alumina support; and 1.07, 1.96, and 0.25%, respectively, in the silica gel support. The results proved that the three load elements were successfully loaded into the carrier.

TABLE 1 | BET data of different catalyst and carriers.

Carrier material	BET surface area (m^2/g)	Pore volume (cm^3/g)
Mn/Mg/Ce@ATP	1,836.143	0.496
Mn/Mg/Ce@MS	388.998	0.952
Mn/Mg/Ce@Al_2O_3	175.111	0.732
Mn/Mg/Ce@SG	95.000	0.277
ATP	408.952	0.471
MS	920.561	0.750
Al_2O_3	516.285	1.96
SG	348.235	0.643

The XRD patterns of Mn/Mg/Ce catalyst are shown in **Figure 2A**. The diffraction peaks at 2θ = 46.149° and 66.881° are consistent with the characteristic peaks of MgO in the JCPDS standard card, and there are obvious peak patterns in the figures of ATP and MS carriers. According to the reference (Li et al., 2020), when the diffraction Angle is 28.68° and 28.7°, the characteristic peaks correspond to the amorphous pair of MnO_2 and crystalline Ce_2O_3, respectively. The characteristic peaks of MnO_2 and Ce_2O_3 are reflected in the XRD patterns of the four carriers, but the intensity of MgO diffraction peaks detected in Al_2O_3 and SG is weak and the peak values are offset, which may be related to the loading amount and crystallization effect. It can be seen from **Figure 1C** that the loading of each element of ATP and MS is larger than that of alumina and SG, and the target element loading is too small, which leads to the weak intensity of target characteristic peak of Al_2O_3 and SG, and there is no obvious characteristic peak in the XRD characterization diagram.

As shown in **Table 1**, Except attapulgite, the specific surface area of the catalyst decreased after calcination, which indicates that the target elements are loaded on the carrier surface, and high-temperature calcination makes the micropores on the carrier surface collapse, particles agglomerate and the specific surface area decrease. Among the four catalysts, the maximum specific surface area of Mn/Mg/Ce@ATP reached 1836.143 m^2/g, and the specific surface area of Mn/Mg/Ce@ATP increased three times than that of ATP. This finding is consistent with the complexity of surface features shown in the SEM results.

Effect of Different Element Doping on Ozone Catalytic Oxidation

The optimum experimental conditions were determined by the degradation of methyl orange wastewater. The treatment effects of the different carriers are shown in **Figure 2B**. The degradation efficiency of the ozone-catalyzed oxidation of methyl orange wastewater was 31.2%. The addition of silica gel carrier increased the degradation rate of methyl orange by 10.4% compared with that of pure ozone oxidation, whereas the impregnation and loading of Mg and Mn increased the degradation rate of methyl orange by 19.6% compared with that of pure ozone oxidation. The addition of Mg and Mn improved the mass transfer efficiency of ozone-catalyzed oxidation. The Mg and Mn concentrations in the impregnation solution remained unchanged. In comparison, the degradation rate of methyl orange reached 96% and the efficiency of ozone catalytic oxidation greatly improved after the addition of 5% $Ce(NO_3)_3$ solution. The experiments showed that the carrier and impregnation elements improve the degradation rate of methyl orange wastewater, and the performance of the catalyst greatly improved after cerium impregnation. This may be in the process of ozone catalytic oxidation, the valence changes of Mn and Ce accelerate the electron transfer in the reaction, so as to improve the ozone catalytic efficiency (Gopi et al., 2016).

Effect of Different Carriers on Catalytic Ozone Oxidation

The treatment effects of catalysts with different carriers are shown in **Figure 2C**. Molecular sieve, attapulgite, nano alumina, and silica gel were impregnated into the same impregnation solution with the same volume. **Figure 2C** illustrates that the degradation rate of methyl orange increased with the increase in cerium doped into the four carriers, which proves that cerium plays a synergistic role in ozone catalytic oxidation. The reason for the difference of treatment effect is that on the one hand, as shown in **Figure 1C**, the target element loading of each catalyst is different. The target element loading of MS is three times that of SG. As a result, the number of reactive active sites on the catalyst surface is different. When the target element content is higher, the more reactive active sites, the better the sewage treatment effect. On the other hand, the BET results of the four catalysts show that the specific surface areas of the catalysts are different. When the specific surface area is larger, it is easier to adsorb organic pollutants in water, so as to improve the efficiency of ozone catalytic oxidation.

Effect of pH on Catalytic Oxidation of Ozone

The pH value of the experimental system directly changes the total concentration of OH, which affects the catalytic activity for the heterogeneous catalytic ozonation of printing and dyeing wastewater. The effects of catalytic ozonation at pH 3, 5, 7, 9, and 11 were investigated in the reaction time of 120 min. **Figure 2D** shows that when the pH values were 3, 5, 7, 9, and 11, the degradation rates of methyl orange wastewater after 120 min of reaction were 78.3, 88, 86, 84.9, and 90.5%, respectively. The highest degradation rate was attained at pH 11. It can be seen from the results that the catalytic oxidation effect of ozone is better under alkaline conditions, because OH plays the main oxidation role at this stage. When the wastewater is acidic, H^+ in the water will consume OH, resulting in the decline of catalytic efficiency. Under alkaline conditions, it will promote the release of OH and enhance the catalytic oxidation of ozone (Salla et al., 2018).

Effect of Catalyst Dosage on Ozone Catalytic Oxidation

The relationship between the catalyst amount and methyl orange degradation rate is shown in **Figure 2E**. The effect of the catalyst concentrations of 1, 2, 3, 4, and 5 g/L on catalytic ozonation within the reaction time of 120 min were determined. When the catalyst dosage was 1, 2, 3, 4, and 5 g/L, the degradation rates of methyl orange wastewater after 120 min were 70.8, 82.3, 87.5,

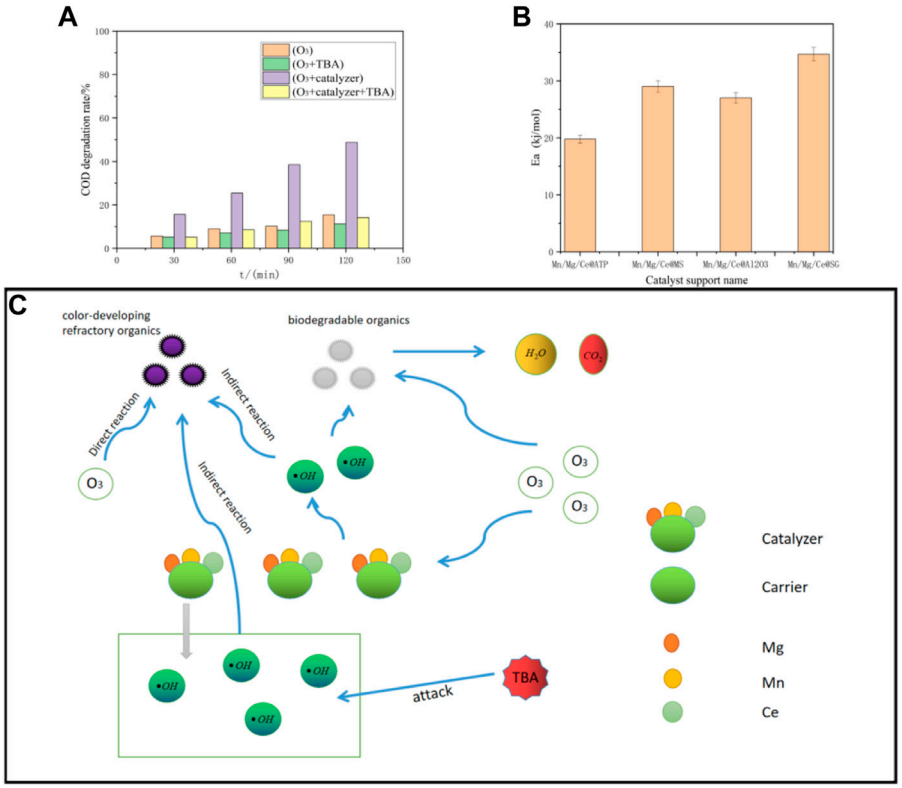

FIGURE 3 | (A) Histogram experiment data of radical quenching experiment in red powder wastewater. **(B)** Graph of activation energy of four supported catalysts. **(C)** Mechanism diagram of ozone catalytic oxidation.

93.8, and 96%, respectively. The highest value was obtained at the catalyst dosage of 5 g/L (Shahamat et al., 2014).

Catalytic Ozonation of Printing and Dyeing Wastewater

Under the optimum conditions (reaction time, 120 min; ozone dose, 36 ppm; pH, 11; and catalyst dose, 5 g/L), the Mn/Mg/Ce catalysts prepared with four different carriers were used in the ozone catalytic oxidation of red powder wastewater. As shown in **Figure 2F**, the COD degradation rate of red powder wastewater was the highest (48.7%) when ATP was used as the carrier, followed by molecular sieve (39.6%), alumina (37.1%), and silica gel (32.5%). According to the results, the catalysts have strong degradation ability for single dye substances in ozone catalytic oxidation and have a certain treatment effect for red powder wastewater with complex components, high COD, and toxicity. Low levels of ozonation raised the BOD_7-concentration of the wastewater plant treated water. However, larger ozone dosages caused the BOD_7 levels to decrease (Sallanko and Okkanen, 2009).

Discussion on the Mechanism of Ozone Catalytic Oxidation

Hydroxyl radical plays an important role in the heterogeneous catalytic oxidation of ozone. Ozone catalysis involves OH oxidation (Ikhlaq et al., 2012). A Mn/Mg/Ce ternary ozone catalyst was adopted in the present study to improve methyl orange degradation rate and COD removal rate in printing and dyeing wastewater. Metal oxide-supported catalyst provides a large number of active centers on the support surface and promotes OH generation (Salla et al., 2018; Unal Yesiller et al., 2012; Ziylan-Yavaş and Ichikawa, 2017). When the pH value of the wastewater is close to the pH value of the catalyst, the surface hydroxyl in neutral state is conducive to produce more OH (Roshani et al., 2014; Wang et al., 2011). **Figure 3A** shows the influence of hydroxyl radical quenching after TBA addition on COD removal rate. Compared with single ozonation, Mn/Mg/Ce ternary ozonation catalyst promotes the formation of hydroxyl radicals and plays a leading role in ozonation. In catalytic ozonation system, the active center on the catalyst surface promotes the decomposition of ozone and produces a large number of highly active hydroxyl radicals to oxidize organic pollutants. (Sui et al., 2010; Vittenet et al., 2015; Wang et al., 2016).

The activation energies of the four catalysts were calculated according to the Arrhenius formula to elucidate the specific catalytic mechanism of the catalyst:

$$K = Ae^{-\frac{Ea}{RT}}, \tag{1}$$

$$\ln K = \ln A - \frac{Ea}{RT}. \tag{2}$$

The reaction activation energies of the four catalysts shown in **Figure 3B** were calculated according to Arrhenius formula. The activation energy of the four carrier's catalysts is in the order: Mn/Mg/Ce@SG > Mn/Mg/Ce@MS > Mn/Mg/Ce@Al_2O_3 > Mn/Mg/Ce@ATP. The catalysts effectively reduced the activation energy of the reaction. The catalyst with lower activation energy can more easily decompose the ozone and has better effect in ozone catalytic oxidation. Among the four catalysts, Mn/Mg/Ce@ATP had the best effect on the ozone catalytic oxidation of dye wastewater.

In this experiment, different carrier catalysts show different ozone catalytic oxidation performance. On the one hand, due to the different properties and specific surface area of the carrier itself, the load of different carriers for target elements is different, which affects the number of overall reaction active sites and the adsorption effect of organic compounds in wastewater. On the other hand, different carriers also promote the catalytic oxidation of ozone, and the synergy intensity after loading target elements is different. For example, Al_2O_3 can be used as a catalyst for ozone catalytic oxidation.

CONCLUSION

The Mn/Mg/Ce catalyst was obtained by the impregnation and calcination of the precursor solution containing Mn, Mg, and Ce compounds. The SEM images show that the active components were obviously attached to the surface of the carrier. The BET surface area data show that a carrier with a larger specific surface area can better load the target elements under the same impregnation conditions. In this study, the catalyst was applied to the catalytic ozonation of printing and dyeing wastewater for the first time.

The catalytic performance of the Mn/Mg/Ce catalyst was studied by simulated dynamic test. The optimum treatment conditions were as follows: reaction time, 120 min; ozone dose, 36 ppm; pH, 11; catalyst dose, 5 g/L; and carrier, attapulgite. Under these conditions, the removal rate of methyl orange reached 96%, and the COD degradation rate of actual printing and dyeing wastewater reached 48.7%. According to the calculation of activation energy, catalyst addition reduced the activation energy of the reaction. Among the four catalysts, the lowest activation energy (E_a = 19.770 kJ/mol) and the best treatment effect on printing and dyeing wastewater were obtained by attapulgite.

The large number of hydroxyl radicals on the surface of the Mn/Mg/Ce ternary ozone oxidation catalyst provides rich active centers for the reaction, which led to ozone decomposition and greatly promoted the transformation of color-developing macromolecular refractory organics to small molecular organics. The results show that the Mn/Mg/Ce ternary ozone oxidation catalyst can be used as a catalyst for the ozonation of printing and dyeing wastewater with good treatment effect. This method provides a new technical method for practical engineering application.

DATA AVAILABILITY STATEMENT

The original contributions presented in the study are included in the article/supplementary material, further inquiries can be directed to the corresponding author.

AUTHOR CONTRIBUTIONS

SZ: conceptualization, methodology, and writing—original draft. HR: acquisition, methodology, and writing—review and editing. WC: investigation, formal analysis, and supervision. KF: investigation and formal analysis. DW: validation and visualization. CL: investigation and supervision. SJ: supervision and validation. JL: validation and visualization. MZ: validation and visualization.

FUNDING

The work was financially supported by Shandong Provincial Major Scientific and Technological Innovation Project (2020CXGC011203, 2019JZZY020211) and the Natural Science Foundation of Shandong Province (ZR202102280483).

REFERENCES

Akhtar, J., Amin, N. S., and Aris, A. (2011). Combined Adsorption and Catalytic Ozonation for Removal of Sulfamethoxazole Using Fe_2O_3/CeO_2 Loaded Activated Carbon. *Chem. Eng. J.* 170 (1), 136–144. doi:10.1016/j.cej.2011.03.043

Batakliev, T., Tyuliev, G., Georgiev, V., Anachkov, M., Eliyas, A., and Rakovsky, S. (2015). Ozone Decomposition Reaction Overα-Alumina-Supported Silver Catalyst: Comparative Study of Catalytic Surface Reactivity. *Ozone: Sci. Eng.* 37, 216–220. doi:10.1080/01919512.2014.957261

Bian, Z., Feng, Y., Li, H., and Zhan, J. (2020). Fabrication of Ag_3PO_4/TiO_2@ molecular Sieve (MS) Ternary Composites with Remarkably Enhanced Visible Light-Responded Photocatalytic Activity and Mechanism Insight. *Environ. Res.* 190, 109984. doi:10.1016/j.envres.2020.109984

Chen, Z., Zhang, M., Hua, J., Yang, M., Dong, Y., and Cheng, H. (2021). Remarkable Activity of Pd Catalyst Supported on Alumina Synthesized via a Hydrothermal Route for Hydrogen Release of Perhydro-N-Propylcarbazole. *Int. J. Hydrogen Energ.* 46 (15), 9718–9729. doi:10.1016/j.ijhydene.2020.08.168

Cui, H., Qian, Y., Li, Q., Wei, Z., and Zhai, J. (2013). Fast Removal of Hg(II) Ions from Aqueous Solution by Amine-Modified Attapulgite. *Appl. Clay Sci.* 72, 84–90. doi:10.1016/j.clay.2013.01.003

Dai, Q., Wang, J., Chen, J., and Chen, J. (2014). Ozonation Catalyzed by Cerium Supported on Activated Carbon for the Degradation of Typical Pharmaceutical Wastewater. *Separat. Purif. Techn.* 127, 112–120. doi:10.1016/j.seppur.2014.01.032

Deng, F., Qiu, S., Chen, C., Ding, X., and Ma, F. (2015). Heterogeneous Catalytic Ozonation of Refinery Wastewater over Alumina-Supported Mn and Cu Oxides Catalyst. *Ozone: Sci. Eng.* 37 (6), 546–555. doi:10.1080/01919512.2015.1065173

Feng, C., Zhao, J., Qin, G., and Diao, P. (2021). Construction of the Fe^{3+}-O-$Mn^{3+/2+}$ Hybrid Bonds on the Surface of Porous Silica as Active Centers for Efficient Heterogeneous Catalytic Ozonation. *J. Solid State. Chem.* 300, 122266. doi:10.1016/j.jssc.2021.122266

Hayat, A., Shaishta, N., Uddin, I., Khan, M., Mane, S. K. B., Hayat, A., et al. (2021). Molecular Engineering of Carbon Nitride towards Photocatalytic H_2 Evolution and Dye Degradation. *J. Colloid Interf. Sci.* 597, 39–47. doi:10.1016/j.jcis.2021.03.159

He, Y., Wang, L., Chen, Z., Shen, B., Wei, J., Zeng, P., et al. (2021). Catalytic Ozonation for Metoprolol and Ibuprofen Removal over Different MnO_2 Nanocrystals: Efficiency, Transformation and Mechanism. *Sci. Total Environ.* 785, 147328. doi:10.1016/j.scitotenv.2021.147328

Huang, Y., Luo, M., Xu, Z., Zhang, D., and Li, L. (2019). Catalytic Ozonation of Organic Contaminants in Petrochemical Wastewater with Iron-Nickel Foam as Catalyst. *Separat. Purif. Techn.* 211, 269–278. doi:10.1016/j.seppur.2018.09.080

Jeirani, Z., and Soltan, J. (2017). Improved Formulation of Fe-MCM-41 for Catalytic Ozonation of Aqueous Oxalic Acid. *Chem. Eng. J.* 307, 756–765. doi:10.1016/j.cej.2016.08.141

Jiang, H., Zhang, R., Hao, J., Xu, X., Chen, J., Zhang, Y., et al. (2021). Design, Preparation, Characterization, and Application of $Mn_xCu_{1-x}O_y/\gamma$-Al_2O_3 Catalysts in Ozonation to Achieve Simultaneous Organic Carbon and Nitrogen Removal in Pyridine Wastewater. *Sci. Total Environ.* 774, 145189. doi:10.1016/j.scitotenv.2021.145189

Kawasaki, N., Tominaga, H., and Ogata, F. (2013). Development of Actual Dyestuff Wastewater Treatment by Ozone with Carbonaceous Materials Produced from Waste Fiber. *Sen-i Gakkaishi* 69, 125–131. doi:10.2115/fiber.69.125

Li, J., Song, W., Yu, Z., and Li, Q. (2020). Preparation of the Mn-Fe-Ce/γ-Al_2O_3 Ternary Catalyst and its Catalytic Performance in Ozone Treatment of Dairy Farming Wastewater. *Arabian J. Chem.* 13 (2), 3724–3734. doi:10.1016/j.arabjc.2020.01.006

Li, X., Chen, W., Ma, L., Wang, H., and Fan, J. (2018). Industrial Wastewater Advanced Treatment via Catalytic Ozonation with an Fe-Based Catalyst. *Chemosphere* 195, 336–343. doi:10.1016/j.chemosphere.2017.12.080

Liu, P., and Guo, J. (2006). Polyacrylamide Grafted Attapulgite (PAM-ATP) via Surface-Initiated Atom Transfer Radical Polymerization (SI-ATRP) for Removal of Hg(II) Ion and Dyes. *Colloids Surf. A: Physicochemical Eng. Aspects* 282-283, 498–503. doi:10.1016/j.colsurfa.2006.02.052

Lun, M., Zhou, X., Hu, S., Hong, Y., Wang, B., Yao, A., et al. (2021). Ferroelectric $K_{0.5}Na_{0.5}NbO_3$ Catalysts for Dye Wastewater Degradation. *Ceramics Int.* 47 (20), 28797–28805. doi:10.1016/j.ceramint.2021.07.040

Madzokere, T. C., and Karthigeyan, A. (2017). Heavy Metal Ion Effluent Discharge Containment Using Magnesium Oxide (MgO) Nanoparticles. *Mater. Today Proc.* 4 (1), 9–18. doi:10.1016/j.matpr.2017.01.187

Mansouri, L., Sabelfeld, M., Geissen, S.-U., and Bousselmi, L. (2013). Catalytic Ozonation of Model Organic Compounds in Aqueous Solution Promoted by Metallic Oxides. *Desalination Water Treat.* 53 (4), 1–12. doi:10.1080/19443994.2013.860630

Martins, R. C., and Quinta-Ferreira, R. M. (2009). Screening of Ceria-Based and Commercial Ceramic Catalysts for Catalytic Ozonation of Simulated Olive Mill Wastewaters. *Ind. Eng. Chem. Res.* 48 (3), 1196–1202. doi:10.1021/ie8006209

Mirilă, D.-C., Boudissa, F., Beltrao-Nuñes, A.-P., Platon, N., Didi, M.-A., Nistor, I.-D., et al. (2020). Organic Dye Ozonation Catalyzed by Chemically Modified Montmorillonite K10- Role of Surface Basicity and Hydrophilic Character. *Ozone: Sci. Eng.* 42 (6), 517–530. doi:10.1080/01919512.2020.1727727

Prabaharan, D. M. D. M., Sadaiyandi, K., Mahendran, M., and Sagadevan, S. (2016). Structural, Optical, Morphological and Dielectric Properties of Cerium Oxide Nanoparticles. *Mat. Res.* 19 (2), 478–482. doi:10.1590/1980-5373-MR-2015-0698

Roshani, B., McMaster, I., Rezaei, E., and Soltan, J. (2014). Catalytic Ozonation of Benzotriazole over Alumina Supported Transition Metal Oxide Catalysts in Water. *Separat. Purif. Techn.* 135, 158–164. doi:10.1016/j.seppur.2014.08.011

Salla, J. S., Padoin, N., Amorim, S. M., Puma, G. L., and Moreira, R. F. P. M. (2018). Humic Acids Adsorption and Decomposition On Mn_2O_3 and α-Al_2O_3 Nanoparticles in Aqueous Suspensions in The Presence of Ozone. *J. Environ. Chem.*. doi:10.1016/j.jece.2018.11.025

Sallanko, J., and Okkanen, J. (2009). Effect of Ozonation on Treated Municipal Wastewater. *J. Environ. Sci. Health* 44 (1), 57–61. doi:10.1080/10934520802515350

Shahamat, Y. D., Farzadkia, M., Nasseri, S., Mahvi, A. H., Gholami, M., and Esrafili, A. (2014). Magnetic Heterogeneous Catalytic Ozonation: a New Removal Method for Phenol in Industrial Wastewater. *J. Environ. Health Sci. Engineer* 12 (1), 50. doi:10.1186/2052-336X-12-50

Sui, M., Sheng, L., Lu, K., and Tian, F. (2010). FeOOH Catalytic Ozonation of Oxalic Acid and the Effect of Phosphate Binding on its Catalytic Activity. *Appl. Catal. B: Environ.* 96 (1-2), 94–100. doi:10.1016/j.apcatb.2010.02.005

Tabrizi, M. T. F., Glasser, D., and Hildebrandt, D. (2011). Wastewater Treatment of Reactive Dyestuffs by Ozonation in a Semi-batch Reactor. *Chem. Eng. J.* 166 (2), 662–668. doi:10.1016/j.cej.2010.11.043

Takahashi, N., Ichikawa, H., Torii, H., Shibata, S., Duy, N. P. H., and Phuong, P. T. T. (2012). Ozonation of Dyestuff Solutions Using a Fine Bubble Generator System. *Ozone: Sci. Eng.* 34, 196–203. doi:10.1080/01919512.2012.663720

Unal Yesiller, S., Eroğlu, A. E., and Shahwan, T. (2012). Removal Of Aqueous Rare Earth Elements (Rees) Using Nano-Iron Based Materials. *J. Industrial Engin. Chem.* 19 (3), 898–907. doi:10.1016/j.jiec.2012.11.005

Vittenet, J., Aboussaoud, W., Mendret, J., Pic, J.-S., Debellefontaine, H., Lesage, N., et al. (2015). Catalytic Ozonation with $_\gamma$-Al_2O_3 to Enhance the Degradation of Refractory Organics in Water. *Appl. Catal. A: Gen.* 504, 519–532. doi:10.1016/j.apcata.2014.10.037

Wang, J. L., and Xu, L. J. (2012). Advanced Oxidation Processes for Wastewater Treatment: Formation of Hydroxyl Radical and Application. *Crit. Rev. Environ. Sci. Techn.* 42, 251–325. doi:10.1080/10643389.2010.507698

Wang, Y., Yang, W., Yin, X., and Liu, Y. (2016). The Role of Mn-Doping for Catalytic Ozonation of Phenol Using Mn/$_\gamma$-Al_2O_3 Nanocatalyst: Performance and Mechanism. *J. Environ. Chem. Eng.* 4 (3), 3415–3425. doi:10.1016/j.jece.2016.07.016

Ziylan-Yavaş, A., and Ichikawa, H. (2017). Catalytic Ozonation Of Paracetamol Using Commercial And Pt-Supported Nano-Composites Of Al_2O_3: The Impact Of Ultrasound. *Ultrason Sonochem.* doi:10.1016/j.ultsonch.2017.02.017

Zhang, M., Yin, D., Guo, J., Wu, H., Gong, M., and Feng, X. (2021). Ternary Catalyst Mn-Fe-Ce/Al_2O_3 for the Ozonation of Phenol Pollutant: Performance and Mechanism. *Environ. Sci. Pollut. Res.* 28 (25), 32921–32932. doi:10.1007/s11356-021-13006-5

Zhang, Y., Yang, H., Zhou, K., and Ping, Z. (2007). Synthesis of an Affinity Adsorbent Based on Silica Gel and its Application in Endotoxin Removal. *Reactive Funct. Polym.* 67 (8), 728–736. doi:10.1016/j.reactfunctpolym.2007.05.003

Zuo, X., Ma, S., Wu, Q., Xiong, J., He, J., Ma, C., et al. (2021). Nanometer CeO_2 Doped High Silica ZSM-5 Heterogeneous Catalytic Ozonation of Sulfamethoxazole in Water. *J. Hazard. Mater.* 411, 125072. doi:10.1016/j.jhazmat.2021.125072

Conflict of Interest: The authors declare that the research was conducted in the absence of any commercial or financial relationships that could be construed as a potential conflict of interest.

Publisher's Note: All claims expressed in this article are solely those of the authors and do not necessarily represent those of their affiliated organizations, or those of the publisher, the editors and the reviewers. Any product that may be evaluated in this article, or claim that may be made by its manufacturer, is not guaranteed or endorsed by the publisher.